Water Air Soil Pollut (2013) 224:1734
DOI 10.1007/s11270-013-1734-7

Nanofiltration of Acid Mine Drainage in an Abandoned Mercury Mining Area

Carlos Sierra · José Ramón Álvarez Saiz · José Luis R. Gallego

Received: 3 May 2013 / Accepted: 26 August 2013 / Published online: 8 September 2013

Abstract In Asturias (north of Spain), mercury mining has been identified as a potential source of trace elements such as As, Sb, Pb, and Hg. In particular, at Los Rueldos mine site, some of these contaminants are dissolved in acidic mine drainage (AMD). Here we treated this leachate by means of nanofiltration to remove some of its pollutants. In order to improve our understanding of the geochemical factors involved in nanofiltration, we analyzed sediment geochemistry and the origin of acidic waters. In coherence with the observation of similar behaviors of As, Fe, and Al in the nanofiltration tests, a clear geochemical association between As, Sb, S, and Fe both in sediments and in the occurrence of AMD was detected. The FILMTEC™ *NF-2540 membrane* used in this study proved to be highly suitable for the treatment and concentration of the metallic and semimetallic contaminants in the acidic water, even at low pH and moderate pressures.

Keywords Nanofiltration · Acid mine drainage · Mercury mining · Arsenic pollution

C. Sierra · J. L. R. Gallego (✉)
Environmental Biotechnology and Geochemistry Group,
C/Gonzalo Gutiérrez Quirós s/n, 33600 Mieres,
Asturias, Spain
e-mail: jgallego@uniovi.es

J. R. Álvarez Saiz
Department of Chemical and Environmental Engineering,
University of Oviedo,
33071 Oviedo, Asturias, Spain

1 Introduction and Objectives

Environmental issues in metal mining sites usually concern the presence of mining effluents and acid mine drainage (AMD). The latter has been reported to be one of the most severe environmental problems caused by mining (Sheoran and Sheoran 2006). AMD has a low pH and an abundance of sulfates and dissolved metals, which can heavily contaminate both surface and groundwater, in addition to soils (Blodau 2006). AMD formation can arise by the oxidation of many types of minerals, although pyrite plays the major role. The oxidation of this mineral is a complex process involving both chemical and biological mechanisms. Nevertheless, these can be simplified in three basic steps. First, pyrite is oxidized, according to Blodau (2006):

$$2FeS_2(s) + 7O_2(g) + 2H_2O(l) \rightarrow 2Fe^{2+}(aq) + 4SO_4{}^{2-}(aq) + 4H^+(aq)$$

The oxidation of sulfide to sulfate solubilizes Fe^{2+}, which is subsequently oxidized to Fe^{3+}:

$$4Fe^{2+}(aq) + O_2(g) + 4H^+(aq) \rightarrow 4Fe^{3+}(aq) + 2H_2O(l)$$

The Fe^{3+} ions produced can precipitate:

$$Fe^{3+}(aq) + 3H_2O(l) \rightarrow Fe(OH)_3(s) + 3H^+(aq)$$

or oxidize additional pyrite, forming supplementary Fe^{2+} cations:

$$FeS_2(s) + 14Fe^{3+}(aq) + 8H_2O(l) \rightarrow 15Fe^{2+}(aq) + 2SO_4{}^{2-}(aq) + 16H^+(aq)$$

The entire process is very slow, and microorganisms such as *Thiobacillus ferrooxidans* catalyze the reaction. As a result of the process, H^+ ions are released, thus lowering the pH and maintaining the ferric ions, heavy metals (Hg, Pb, Zn, etc.), and metalloids (As, Sb, Se) in solution (Johnson and Hallberg 2003).

AMD can be remediated by means of either chemical or biological mechanisms. These systems can be classified as active, when they require continuous reactive addition once in operation, or passive, when relatively small amounts of resources are needed to sustain the process. Apart from off-line sulfidogenic bioreactors, most biological remediation processes for AMD are passive systems (Johnson and Hallberg 2005). Among the active techniques, the addition of alkaline materials, combined with the addition of oxidizing agents that promote the precipitation of metals as hydroxides and/or carbonates, has been extensively used for AMD treatment (Kuyucak 2001, 2002).

However, these techniques have the following disadvantages:

- They may require large doses of reagents to maintain the desired pH for the precipitation of the metal (Matlock et al. 2002).
- They generate secondary waste (such as metal hydroxides or gypsum), which should be treated again, conditioned, or disposed of in a landfill next to the mining areas, thus increasing the risks and costs during storage (Harris and Ragusas 2001).
- They lack selectivity for the recovery of target species, thereby hampering the possibility of an economic recovery of the metal (Johnson and Hallberg 2005).

Although more intensive in energy and cost, other experimental active technologies have been proposed in recent years to overcome these limitations. These include solvent extraction (Stevanović et al. 2009), ion exchange (Gaikwad et al. 2010), adsorption (Motsi et al. 2011), as well as membrane technologies. The latter involve several strategies in which the driving force is a pressure gradient, such as ultrafiltration, nanofiltration, and reverse osmosis, and their use has been reported only for very few cases (see, for example, Mason and Gupta (1972), Zhong et al. (2007), Al-Zoubi et al. (2010)). Membrane technologies offer a number of advantages; they show adaptability to changes in flow characteristics (concentration of heavy metals, temperature, etc.) in order to provide high recovery of dissolved metals and can be used to preconcentrate valuable metals contained in the leachate that can then be reclaimed. In addition, they have low operating times and a modular design and are easy to use (Rautenbach and Gröschl 1990). The main disadvantages are the relatively high operating costs and the risk of membrane fouling caused by the precipitation of calcium sulfate.

Given the presence of hazardous trace elements such as As, Pb, and Hg, abandoned mercury mines and metallurgy facilities in Asturias (northern Spain) are a potential source of pollution (Loredo et al. 1988; Baldo et al. 1999). In this regard, soil, sediment, and water pollution, together with an active AMD, have been detected in one of the mercury mines ("Los Rueldos") in the abovementioned region (Loredo et al. 2005).

The present study aims to (a) provide an overview of the environment in which the AMD in Los Rueldos was formed, reporting data from the geochemistry of the sediments and parental rocks; (b) assess the rates of removal of As, Al, Fe, and SO_4^{2-} ions contained in the AMD by nanofiltration as a prelude to a pilot-scale test; and (c) offer insight into the theoretical models applicable to this kind of separation in AMD.

2 Materials and Methods

2.1 Site Description

The samples were collected in the mining district of Mieres in Asturias, which, together with Pola de Lena, in the same region, was Spain's second largest Hg mining district after Almadén (Luque 1985). Los Rueldos is a pyrite-rich mine deposit like those widely exploited to obtain chalcophile metals (Au, Ag, Hg, Cu, Zn, Pb, etc.). It is located on the northwestern slope of the valley of the Morgao stream, approximately 2 km to the northeast of the town of Mieres and 20 km to the southeast of Oviedo (northern Spain). Mining activities ceased in 1972.

Mercury mining and metallurgy activities in this area included the exploitation of the Hg-rich ores consisting mainly of cinnabar, and accompanied by other minerals such as arsenopyrite, rejalgar, sphalerite, As-rich pyrite, marcasite, and chalcopyrite. The gangue is fundamentally quartz, with the presence of carbonates, in the form of calcite, dolomite, and

ankerite, and argillaceous minerals such as kaolinite and dickite (Luque et al. 1989).

The mining activities generated the disposal of vast volumes of gangue minerals that are affected by mechanical and chemical dispersion and weathering, thus releasing large amounts of heavy metals into the environment (Sierra et al. 2011). In fact, significant concentrations of Pb, Hg, Fe, and especially As have been reported (Loredo et al. 2005).

In particular, one of the disused galleries shows a permanent effect of AMD, namely alteration of the materials in the environment, thus favoring the activity of Fe-oxidizing acidophilic bacteria. This alteration has led to a flow of lixiviates running over sediments in both the mine gallery and in the pond at its entrance.

2.2 Sediment Sampling

Several areas of interest were identified after initial in situ measurements. We then performed a double sampling campaign. In a prospective campaign, and in order to perform a multi-element characterization, we collected samples at 30 points randomly located in the area, from a depth between 0 and 30 cm, using a Dutch auger.

In the second campaign, a "macrosample" of about 50 kg (from an area representative of the average data found in the prospective campaign) was taken from superficial sediments with stainless steel hand augers and shovels from the tilled depth (0–30 cm) and stored in an inert plastic bag. This sample was used to study the distribution of the contaminants in the distinct grain-size fractions.

2.3 Sediment Analysis and Grain-Size Distribution Determination

All sediment samples subjected to chemical characterization were oven-dried for 48 h at a temperature below 40 °C to minimize the loss of Hg, as this metal is highly volatile. After drying the samples, vegetation and other nonsediment materials (including rocks, gravel, and particles greater than 5 mm) were hand-removed prior to homogenization. Samples were then thoroughly disaggregated, mixed, and passed through a 4-mm aperture stainless steel sieve. Afterwards, a representative amount of this fraction was ground in a vibratory disc mill (RS 100 Retsch) at 400 rpm for 40 s to reduce the grain size to below 125 μm. Finally, the ground material was homogenized and quartered to provide a 1-g representative subsample for chemical analysis.

Samples subjected to grain-size characterization were wet-sieved in cycles of 100 g for 5 min with a water flow of 0.3 L/min (ASTM D-422-63, Standard Test Method for Particle-Size Analysis of Soils) into the normalized particle-size fractions of <63, 63–125, 125–250, 250–500, 500–1,000, 1,000–2,000, and 2,000–4,000 μm. The fractions were recovered with the help of a spray nozzle and then ground (when necessary as abovementioned) and analyzed.

For chemical analysis, 1-g representative subsamples were attacked by means of an "aqua regia" digestion ($HCl+HNO_3$) and subsequently analyzed by inductively coupled plasma optical emission spectrometry (ICP-OES) at Activation Laboratories Ltd. (Actlabs), in Ancaster, Ontario (Canada). Actlabs is an ISO 17025 (Lab 266)- and NELAP (Lab E87979)-accredited lab for specific registered tests.

2.4 Multivariate Statistics

In order to study the geochemical behavior of the elements in the sediment, we carried out a cluster analysis of the multi-element data obtained after the prospective campaign. This analysis was done using Ward's algorithm, which maximizes the variance between groups and minimizes it between members of the same group (Gallego et al. 2002). A dendrogram obtained with the statistical software SPSS v18.0 was used to show the clustering of results. Groups of elements with a similar geochemical behavior were identified on the basis of the statistical distance between them (squared Euclidean distance was selected).

2.5 Water Characterization

Samples from the AMD ponds at the entrance of the main gallery were taken weekly for 3 months during the spring of 2011. Subsamples were passed through a Sartorius membrane filter with 0.45-μm pore size; the first few milliliters were used for rinsing and then discarded, and the filtrate was transferred to clean polyethylene bottles and stored at 4 °C. Multi-element analysis was performed by means of inductively coupled plasma mass spectrometry (Perkin Elmer-Sciex, Elan 6000) and ion analyses by ion chromatography (IC 883 Basic plus, Metrohm). The pH, redox potential, conductivity, and dissolved oxygen

were measured in situ by means of a multimeter Multi 340i/SET (WTW) in various sections of the mine gallery, as well as in the pond at the entrance. The remaining of the solution from the AMD pond samples was filtered and mixed together to provide a composite solution of 38 L. This composite sample was stored at 4 °C before being used for the filtration experiment.

2.6 Membrane Separation Experiments

The composite sample was treated with the NF2540 membrane. Designed for the treatment of brackish water, the removal of organic compounds, acidic solution processing, and metal recovery, among other applications, this membrane is made of amide polypiperazine and is low fouling and low energy consuming, thus increasing its lifetime and the time between cleaning periods, compared to other membranes (Applied Membranes, Inc. 2013).

The experimental nanofiltration apparatus consisted of a test rig, with a feed tank, a positive displacement three-plunger pump, the membrane module, a pressure-regulating needle valve, a retentate flowmeter, and pressure (before and after the module) and temperature sensors (Fig. 1).

First of all, distilled water was used to determine membrane permeability and establish the clean membrane conditions. Next, the membrane module was fed with the AMD solution to check membrane performance at several transmembrane pressures (TMP; 5 to 30 bar). In this experiment, called pressure–flux, retentate and permeate are returned to the feed tank, so the concentration of species is constant. Permeate flux is measured by accounting for the filtered volume per time and per unit surface area of the membrane, and rejection gives the selectivity of the membrane for solutes, given by the expression:

$$R = 1 - C_P \Big/ C_R \tag{1}$$

C_P being the concentration of the solute in the permeate and C_R the concentration of solute in the retentate.

Samples from the permeate and the retentate were taken simultaneously and subsequently subjected to chemical analysis following the procedures described in Section 2.5.

Membrane performance can be explained using the solution–diffusion model (Lonsdale et al. 1965), where two coefficients, A and B, can be derived from experimental data.

A and B are the solvent and solute permeabilities, respectively, assuming that both dissolve into the membrane material and are transported by diffusion to the permeate. Permeate flux (productivity) and membrane rejection (selectivity) can be predicted using operating parameters such as the transmembrane pressure, and solute concentration using osmotic pressure. The basic equations are:

$$J = A(\Delta P - \Delta\pi) \tag{2}$$

where J is the solvent flux (water in this case), A is the water permeability, ΔP is the operating transmembrane pressure, and $\Delta\pi$ is the osmotic pressure difference between the retentate and the permeate, and:

$$J_S = JC_P = B(C_R - C_P) \tag{3}$$

where J_S is the solute flux, B is the solute permeability, C_P is the concentration of the solute in the permeate, and C_R is the concentration of the solute in the retentate.

From these two parameters and the definition of rejection in Eq. (1), the rejection can be predicted with the A and B parameters and the operating variables:

$$R = A(\Delta P - \Delta\pi) \Big/ [A(\Delta P - \Delta\pi) + B] \tag{4}$$

A concentration experiment was carried out at a constant transmembrane pressure of 20 bar and a retentate flow of 1,000 L/h. In this experiment, only the retentate is returned to the feed tank while the permeate is continuously removed. This approach allows assessment of the solute concentration. The experiment is followed by taking samples of the permeate and retentate at a range of concentrations, accounting for the volume removed from the system. A volume reduction factor (VRF), defined as the ratio of the initial volume (V_0) and the remaining volume in the system, is used to monitor the experiment. The remaining volume is actually the initial volume minus the volume removed as permeate by filtration (VF):

$$VRF = V_0 \Big/ (V_0 - VF) \tag{5}$$

Considering that the transport of solute depends on the convection of solutes to the boundary layer next to the membrane, and taking into account that the

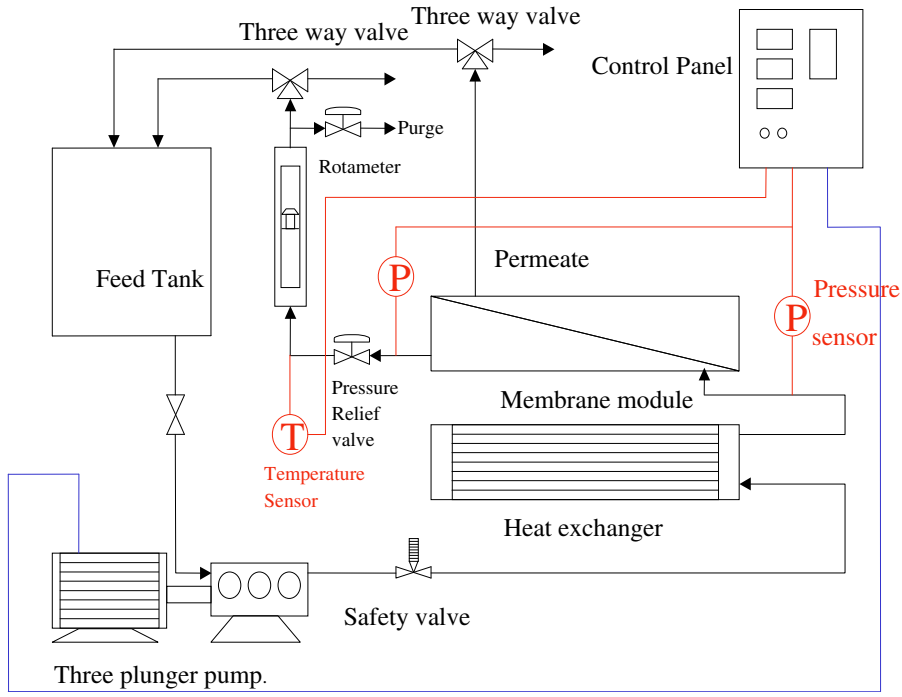

Fig. 1 Flow diagram of the experimental equipment

membrane selectively rejects solutes, there is a concentration of solids next to the membrane surface. This accumulation induces a back diffusion of solutes from the boundary layer to the bulk of the solution. This implies that at steady state the transport equation can be expressed as:

$$J = K \ ln \ (C_M - C_P) \Big/ (C_B - C_P) \quad (6)$$

where J is the solvent flux, K is a mass transfer coefficient, and C_M is the maximum concentration for the solution that will give no flux. Sometimes it is referred to as the gel concentration (especially for food streams).

3 Results and Discussion

3.1 Sediment Characterization Results

Sulfide-rich and low carbonate content in the rock matrix coupled with a significant low content of alkaline material reflects the potential of the site to generate AMD (Table 1). The As concentrations were remarkable, irrespective of the origin of the samples, and fluctuations in the concentration of this metalloid appeared to be correlated with Sb. In contrast, other trace elements, such as Zn or Pb, did not show the same behavior.

The detailed analysis of the grain-size fractions of the 50-kg sediment sample are shown in Table 2. A clear enrichment in trace metals can be observed in fine fractions (especially in those below 250 μm), for instance, for Hg or Pb maximums were found in the fraction below 20 μm, while for As top contents were present in the grain size between 63 and 250 μm. This different behavior could be attributed to the dissimilar mobility of these elements and the variety of weathering phenomena taking place on the abandoned mining area. Unlike elements in the interior of a rock matrix, those present in fine-grained materials, which have larger specific surfaces and hence are more reactive, are easier to release.

As expected, larger particles contained, on a weight basis, considerably less contaminant than the smaller ones. Nevertheless, no fraction presented As concentrations lower than 5,000 mg/kg; concretely, the As content in fractions above 1 mm were associated with the origin of the pollution, namely the chemical and

Table 1 ICP-OES analysis of 30 sediment samples in the study area

Element	Units	Detection limit	Minimum	Maximum	Average	Std. deviation
Al	%	0.01	0.22	1.26	0.57	0.28
As	mg/kg	10	68	62,196	17,743	15,147
Ca	%	0.01	<0.01	1.39	0.31	0.31
Cd	mg/kg	0.5	0.2	4.1	0.7	0.7
Co	mg/kg	1	1	81	18	20
Cr	mg/kg	2	11	134	30	23
Cu	mg/kg	1	12	596	61	106
Fe	%	0.01	2.10	12.40	6.14	2.75
Hg	mg/kg	1	7	2,224	165	432
K	%	0.01	0.04	1.77	0.20	0.29
La	mg/kg	1	3	14	8	3
Mg	%	0.01	<0.01	0.31	0.09	0.08
Mn	mg/kg	2	2	2,320	478	559
Na	%	0.01	<0.01	0.07	0.03	0.02
Ni	mg/kg	1	3	120	32	31
P	mg/kg	0.001	<0.001	0.008	0.005	0.002
Pb	mg/kg	2	19	22,667	1,250	3,918
S	%	0.01	0.16	3.74	0.83	0.71
Sb	mg/kg	10	13	17,396	920	3,212
Sr	mg/kg	1	19	118	51	27
Zn	mg/kg	1	5	429	67	83

physical weathering of the ore rocks biologically catalyzed (at first sight, particles of pyrite and arsenopyrite were observed in the site). This implies that the distribution of elements was regular regardless of the sediment fractions and therefore not controlled only by the binding of trace elements to clays and organic matter, as usually happens. To complement the information obtained, a multivariate study of the chemical results was performed. The main conclusions are summarized in the dendrogram shown in Fig. 2.

The dendrogram depicts three main groups of elements (one of them subdivided into two):

Table 2 Textural distribution and concentration of selected elements after wet sieving of particles <4 mm (maximum values are indicated in italics) for some sediment samples

Particle size (μm)	% over total weight	Chemical analysis of some selected elements					
		Fe (%)	Hg (mg/kg)	As (mg/kg)	Pb (mg/kg)	Zn (mg/kg)	Sb (mg/kg)
4,000–2,000	39.77	5.17	7	6,910	24	35	10
2,000–1,000	14.78	6.81	7	8,190	29	43	16
1,000–500	9.14	8.09	9	11,100	47	46	20
500–250	6.68	9.29	9	14,100	53	56	26
250–63	9.64	*10.30*	12	*16,400*	81	63	29
63–40	1.96	9.97	15	15,800	129	*429*	*32*
40–20	3.37	9.29	15	14,400	110	187	30
<20	14.93	8.05	*23*	11,600	*193*	179	27

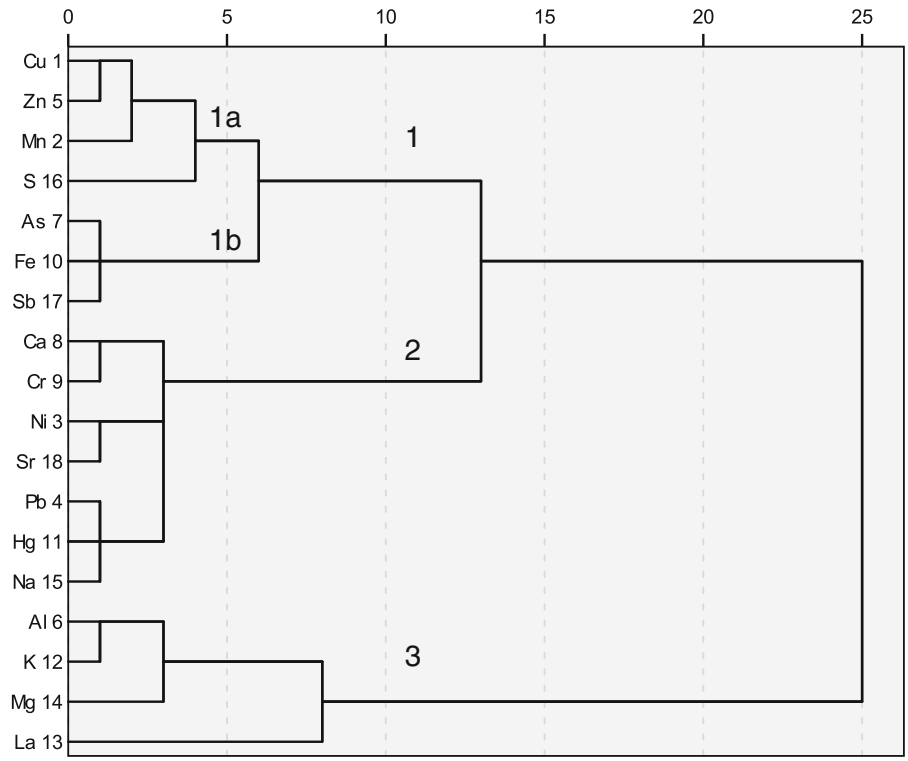

Fig. 2 Dendrogram showing clustering of elements associated by their geochemical affinity within the samples. Main groups are indicated

- Group 1: Comprises chalcophile elements and is subdivided into two subgroups. Subgroup 1a includes Cu, Zn, and Mn, whereas subgroup 1b includes As, Fe, and Sb. The components of subgroup 1b are clearly correlated with the mineral composition of the ores (see Loredo et al. 2005), in which the presence of As-rich pyrite and arsenopyrite has been reported. These minerals are clearly the origin of the Fe and sulfate-rich drainage, which is most probably enhanced by the biocatalyzed oxidation of all the sulfur minerals exposed to weathering within the old mine. In fact, secondary minerals such as goethite, limonite, jarosite, gypsum, and others, including elements belonging to groups 1 and 2 (see below), can be observed in the local paragenesis of the ore body.
- Group 2: Linked to group 1, it includes the rest of the main pollutants in the site (Hg and Pb), thereby indicating the effects of physical weathering of galena and cinnabar, more than chemical weathering, which, in this case, can be linked to the As associated with the chemical oxidation of pyrite minerals.
- Group 3: Statistically very far from the preceding groups. Comprises elements linked to the alteration of the gangue rocks (Al, K, Mg as major components of clay, sands, etc.).

Table 3 Chemical composition of the initial composite sample

	Fe	Al	As	Hg	Pb	Li^+	Na^+	NH_4^+	K^+	Ca^{2+}	Mg^{2+}	SO_4^{2-}	Cl^-	F^-
mg/L	723	147.8	7.2	5×10^{-5}	4.03×10^{-3}	0.133	5.537	0.053	1.763	88.059	37.465	2,360.1	96.7	2.2

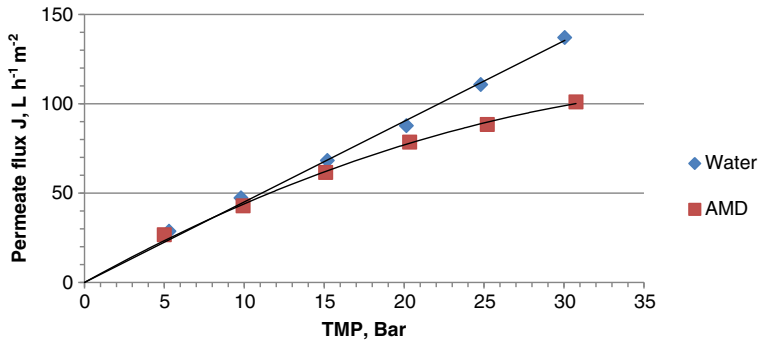

Fig. 3 Effect of TMP in the permeate flux (*J*)

3.2 Geochemical Parameters of the Water

As expected, significant amounts of heavy metals were found in the AMD, as their presence in this drainage is associated with leaching of the heavy metals contained in source rocks and sediments.

In this regard, in samples taken from the AMD pool and at the entrance of the main gallery, the pH was 2.47, the average redox potential was 592 mV, and the dissolved oxygen was 3.3 mg/L. These redox conditions favor the solubilization of inorganic elements from the aforementioned sediments and result in the presence of high concentrations of Fe, Al, As, and sulfates in the water. Thus, chemical analysis of the ten samples taken revealed average concentrations of 2,300 mg/L of sulfate, 6 mg/L of As, 23 mg/L of Al, 515 mg/L of Fe, and 2.3 μg/L of Hg. Given the small size of the evaporative pool at the entrance of the gallery, no significant increase in the concentration of any of these species was observed. The measured values were in accordance with those normally reported for AMD in similar environments (see, for example, Sánchez-España et al. (2005)), and some of them exceeded the environmental standards (see, for example, USEPA Water Quality Criteria (2009) for aquatic environments).

In this regard, the oxidative dissolutions of the pyrite appeared to be responsible for the high concentrations of Fe and SO_4^{2-} in the drainage, while arsenopyrite and realgar accounted for the As, and aluminosilicates like feldspars for the Al. The concentrations of some of the species of environmental concern in the composite sample treated through nanofiltration are shown in Table 3.

3.3 Nanofiltration Results

3.3.1 Pressure–Flux Experiment

Figure 3 shows the effect of operating transmembrane pressure on permeate flux. At the lower pressures tested (up to 10 bar), the filtration rate (permeate flux) was the same as that obtained with water, thus indicating that at the conditions of the effluent there was almost no polarization (which is the concentration of solutes next to the membrane surface and that hinders filtration). Over 10 bar, polarization was observed, and the permeate flux limit was still not reached at 30 bar.

Chemical analysis of the samples taken at different pressures showed that the rejection of metals is high at 5 bar (88 %). Rejection increases with pressure, up to 99 % at 15 bar, remaining at this value at higher pressures. From the pure water data, the membrane permeability (*A*) was 4.647 L/m^2/h/bar. From the data in Table 4, the solute flux (J_S) for each species was obtained. Then, by plotting J_S vs. $C_R - C_P$, the

Table 4 Chemical analysis of metals in the permeate

Pressure (bar)	Concentration (mg/L)			
	Al	Fe	As	SO_4^{2-}
5	18.4	82.0	0.85	670
10	4.0	18.0	0.18	283
15	1.6	7.0	0.07	201
20	1.2	5.9	0.06	184
25	1.3	5.2	0.05	178
30	1.2	5.7	0.06	180

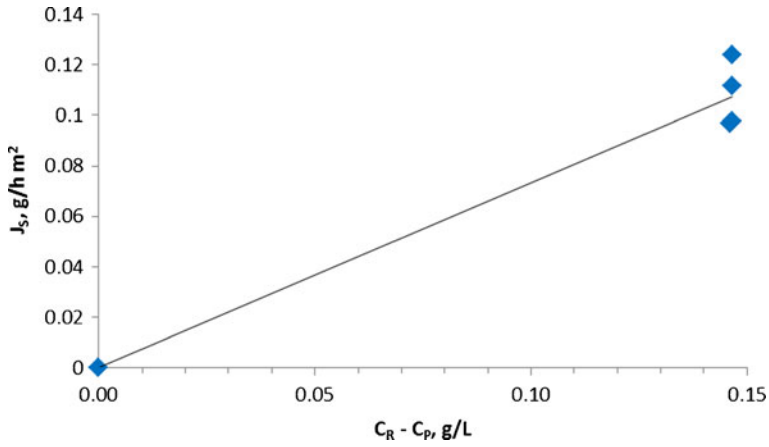

Fig. 4 Solute transport defined as $J_S=B\ (C_R-C_P)$

parameter B was calculated. Figure 4 shows the J_S values for Al. The line fitting of these data gives parameter B, with the same units as A. Aluminum, Fe, and As had the same B value, 0.733 L/m^2/h/bar, while for SO_4^{2-} B was 3.045 L/m^2/h/bar.

The Al and SO_4^{2-} concentrations were below the legal limits for all the permeates whereas As concentrations were below the legal limits at 20 bar, and Fe removal was not possible in a single step.

The rejection for Al, As, and Fe was the same and very high (99 %; Fig. 5). The rejection of the membrane, according to the manufacturer, is 98 % minimum for $MgSO_4$. In this case, there was affinity between Fe, Al, and As, caused by the high adsorption capacity of Fe compounds, which, at pH close to 3, were present in the form of very small oxyhydroxysulfate precipitates with low crystallinity (Bigham and Nordstrom 2000) that fix As and Al onto their surfaces (Langmuir 1997; Smith 1999).

The prediction of the solution–diffusion model using Eq. (4) fitted the experimental data, although predicted rejection values for Al, Fe, and As at lower pressures were higher than the experimental values. This discrepancy is explained by the fact that the fitting of parameter B is obtained by giving more weight to the data at higher pressures.

3.3.2 Concentration Experiment

The experimental results show that from the initial AMD concentration over 99 % of the total content of Al, Fe, and As and around 97 % of the sulfate content were removed by nanofiltration at increasing VRFs.

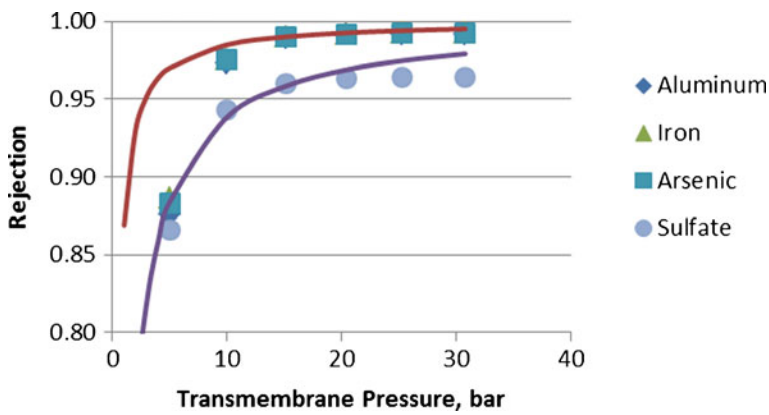

Fig. 5 TMP effect on metal rejection

Table 5 Concentration (mg/L) of major ions at different VRFs

VRF	Al		Fe		As		SO_4^{2-}	
	Perm.	Reten.	Perm.	Reten.	Perm.	Reten.	Perm.	Reten.
1	1.2	148	4.7	723	0.04	7.2	170	4,991
1.17	1.3	176	5.5	839	0.05	8.6	208	6,023
1.4	1.4	210	6.1	1,024	0.06	10.4	251	7,080
1.75	1.6	246	7.4	1,188	0.07	12.3	298	8,322
2	1.9	285	8.6	1,416	0.09	14.2	343	9,264
2.3	2.3	201	10.4	1,020	0.10	10.2	392	1,207
2.8	2.9	413	13.0	2,124	0.13	21.2	470	14,500
3.5	3.7	506	16.5	2,618	0.16	26.1	558	17,083
Final collected permeate	1.7		7.5		0.08		245	

VRF volume reduction factor, *Perm.* permeate, *Reten.* retentate

The concentration of pollutants in the retentate increased as the volume reduction process progressed, thereby indicating acceptable membrane rejection. The concentration of metal in the retentate increased by a factor almost equal to the VRF, thus indicating almost 100 % rejection (Table 5).

Flux decreased with the concentration at a constant transmembrane pressure (Fig. 6). Experimental data at higher concentrations should show a larger decrease in permeate flux; however, the apparatus was unable to maintain the same temperature, and the flux did not decrease in response to a temperature rise in the retentate.

According to the boundary layer mass transfer equation, by plotting permeate flux vs. ($C_R - C_P$), and using log scale for the concentration difference, one should get a straight line with a negative slope, whose numeric value should be the mass transfer coefficient over the boundary layer. As shown in Fig. 6, K should be 23.67 L/h/m^2. The value of ($C_R - C_P$) when J=0 should give the maximum concentration attainable for the solutes, that is ($C_M - C_P$). C_P is negligible because the membrane shows almost 100 % rejection. Therefore, C_M was 1.05 mol/L or an equivalent of 57 g/L. By applying the solution–diffusion model to the data of the concentration experiment, we obtained a curved line, showing a notable decrease in permeate flux as the osmotic pressure of the retentate increased (Fig. 6).

Considering the species individually, all three metals followed the same trend (Fig. 7). This

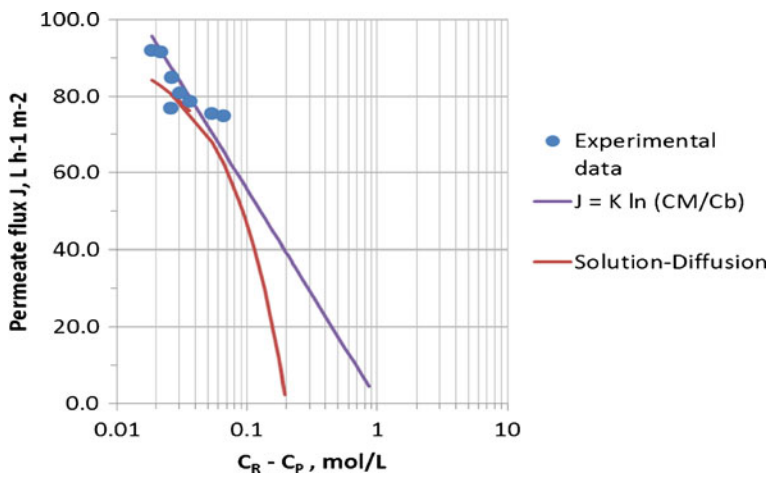

Fig. 6 Effect of concentration on the permeate flux at constant TMP

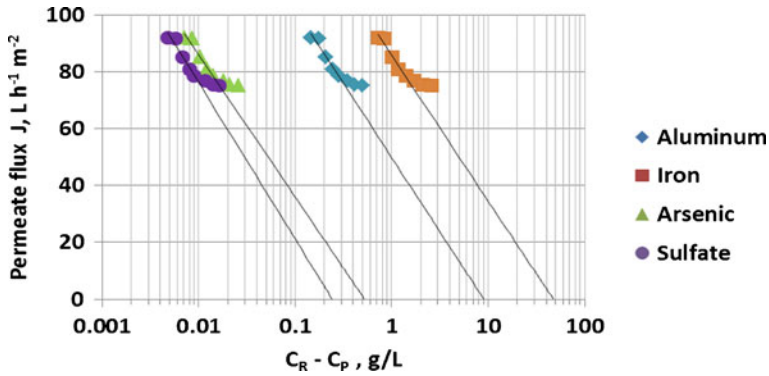

Fig. 7 Effect of concentration of the individual species on the permeate flux

observation indicates that the three species had a strong affinity. SO_4^{2-} showed a slightly different behavior and maximum concentrations differed depending on the species considered: 47.37 g/L for Fe, 9.02 g/L for Al, 0.52 g/L for As, and 0.24 g/L for SO_4^{2-}. In Fig. 7, the effect of an increase in temperature (up to 10 °C) on the permeate flux at higher concentrations as a result of the poor heat exchange capacity of the system is more evident than in Fig. 6.

The pH of the retentate can be later adjusted using calcium hydroxide (lime) to precipitate the metal (hydroxide form) and then be disposed of as solid waste. Although toxicity was reduced in the permeate, this was still too toxic, implying that the nanofiltration treatment should be carried out in at least two stages in order to comply with legal limits for toxicity.

4 Conclusions

Geochemical and mineralogical data from Los Rueldos sediment heap suggest that Fe sulfides enriched in As and left in a humid atmosphere with abundant runoff and bacterial activity are mainly responsible for the high concentrations of As in the surrounding areas.

From a textural point of view, this As was evenly distributed in all grain-size fractions. Multivariate statistical analysis showed a clear affinity between As–Sb–S–Fe, indicating a strong correlation of As with pyrite and Fe oxyhydroxides. In consequence, runoff over these fine-grained sediments, in conjunction with the abovementioned physical, chemical, and biological factors, are responsible for the formation of the AMD.

Many studies have proposed that, in AMD environments, a portion of As is often associated with amorphous Fe oxides and Al. We observed this relationship during the nanofiltration treatment of acidic water samples. Thus, the high content of Fe in acidic waters may facilitate the separation process by scavenging Al and As cations.

In general terms, the membrane used in this study showed high yield and was effective in removing the pollutants even at low pH. Moderate pressures were required for the separation, thus decreasing the costs associated with the process.

References

Al-Zoubi, H., Steinberger, P., Pelz, W., Haseneder, R., & Härtel, G. (2010). Optimization study for treatment of acid mine drainage using membrane technology. *Separation Science and Technology, 45*, 1–13.

Applied Membranes, Inc. (2013) FILMTEC™ Membranes. FILMTEC NF270 Nanofiltration Elements for Commercial Systems. http://www.appliedmembranes.com/pdf/FilmTec%20Specs/NF270-2.5%20&%204Inch.pdf. Accessed 4 Sept 2013.

Baldo, C., Loredo, J., Ordóñez, A., Gallego, J. R., & García-Iglesias, J. (1999). Geochemical characterization of wastes from a mercury mine in Asturias (northern Spain). *Journal of Geochemical Exploration, 67*, 377–390.

Bigham, J. M., & Nordstrom, D. K. (2000). Iron and aluminum hydroxysulfates from acid sulfate waters. In Sulfate minerals: crystallography, geochemistry, and environmental significance (eds. C.N. Alpers, J.L. Jambor and D.K. Nordstrom). *Reviews in Mineralogy and Geochemistry, 40*, 351–403.

Blodau, C. (2006). A review of acidity generation and consumption in acidic coal mine lakes and their watersheds. *Science of the Total Environment, 369*(1–3), 307–332.

Gaikwad, R. W., Sapkal, V. S., & Sapkal, R. S. (2010). Ion exchange system design for removal of heavy metals from acid mine drainage wastewater. *Acta Montanistica Slovaca, 15*(4), 298–304.

Gallego, J. R., Ordóñez, A., & Loredo, J. (2002). Investigation of trace element sources from an industrialized area (Avilés, northern Spain) using multivariate statistical methods. *Environment International, 27*, 589–596.

Harris, M. A., & Ragusas, S. (2001). Biorremediation of acid drainage using decomposable plant material in a constant fow biorreactor. *Journal of Environmental Geology, 40*(20), 1192–1204.

Johnson, D. B., & Hallberg, K. B. (2003). The microbiology of acidic mine waters. *Research in Microbiology, 154*, 466–473.

Johnson, D. B., & Hallberg, K. B. (2005). Acid mine drainage remediation options: a review. *Science of the Total Environment, 338*, 3–14.

Kuyucak, N. (2001). Acid mine drainage—treatment options for mining effluents. *Mining Environmental Management, 9*, 14–17.

Kuyucak, N. (2002). Role of microorganisms in mining: generation of acid rock drainage and its mitigation and treatment. *The European Journal of Mineral Processing and Environmental Protection, 2*(3), 179–196.

Langmuir, D. (1997). *Aqueous environmental geochemistry.* Upper Saddle River: Prentice-Hall.

Lonsdale, H. K., Merten, U., & Riley, R. L. (1965). Transport properties of cellulose acetate osmotic membranes. *Journal of Applied Polymer Science, 9*, 1341.

Loredo, J., Luque, C., & García-Iglesias, J. (1988). Conditions of formation of Hg deposits from the Cantabrian zone (Spain). *Bulletin de Mineralogie, 111*, 393–400.

Loredo, J., Álvarez, R., & Ordóñez, A. (2005). Release of toxic metals and metalloids form Los Rueldos mercury mine (Asturias, Spain). *Science of the Total Environment, 340*, 247–260.

Luque, C. (1985). *Las mineralizaciones de mercurio de la Cordillera Cantábrica*, Ph.D. thesis, University of Oviedo, Spain.

Luque, C., García Iglesias, J., & García Coque, P. (1989). Características geoquímicas de los minerales de mercurio de la Cordillera Cantábrica (NW de España). *Trabajos de Geologia, 18*, 3–11.

Mason, D. G., & Gupta, M. K. (1972). *Reverse osmosis demineralization of acid mine drainage*. Washington, D.C: U.S. Environmental Protection Agency.

Matlock, M. M., Howerton, B. S., & Atwood, D. A. (2002). Chemical precipitation of heavy metals from acid mine drainage. *Water Research, 36*(19), 4757–4764.

Motsi, T., Rowson, N. A., & Simmons, M. J. H. (2011). Kinetic studies of the removal of heavy metals from acid mine drainage by natural zeolite. *International Journal of Mineral Processing, 101*(1–4), 42–49.

Rautenbach, R., & Gröschl, A. (1990). Separation potential of nanofiltration membranes. *Desalination, 77*, 73–84.

Sánchez-España, F. J., López Pamo, E., Santofimia, E., Aduvire, O., Reyes, J., & Baretino, D. (2005). Acid mine drainage in the Iberian Pyrite Belt (Odiel River watershed, Huelva, SW Spain): geochemistry, mineralogy and environmental implications. *Applied Geochemistry, 20*, 1320–1356.

Sheoran, A. S., & Sheoran, V. (2006). Heavy metal removal mechanism of acid mine drainage in wetlands: a critical review. *Minerals Engineering, 19*(2), 105–116.

Sierra, C., Menéndez-Aguado, J. M., Afif, E., Carrero, M., & Gallego, J. R. (2011). Feasibility study on the use of soil washing to remediate the As–Hg contamination at an ancient mining and metallurgy area. *Journal of Hazardous Materials, 196*, 93–100.

Smith, K. S. (1999). Metal sorption on mineral surfaces: an overview with examples relating to mineral deposits. In The environmental geochemistry of mineral deposits, part A: processes, techniques, and health issues: Society of Economic Geologists (eds. G.S. Plumlee and M.J. Losdon), *Reviews in Economic Geology, 6A*, 161–182.

Stevanović, Z., Antonijević, M., Jonović, R., Avramović, L. J., Marković, R., Bugarin, M., et al. (2009). Leach-SX-EW copper revalorization from overburden of abandoned copper mine Cerovo, Eastern Serbia. *Journal of Mining and Metallurgy, 45 B*(1), 45–57.

U.S. Environmental Protection Agency (2009). *National recommended water quality criteria: U.S. Environmental Protection Agency.* Offices of Water and Science and Technology. http://www.epa.gov/ost/criteria/wqctable/. Accessed 4 Sept 2013.

Zhong, C. M., Xu, Z. L., Fang, X. H., & Cheng, L. (2007). Treatment of acid mine drainage (AMD) by ultra-low-pressure reverse osmosis and nanofiltration. *Environmental Engineering Science, 24*(9), 1297–1306.